ACS APPLIED MATERIALS & INTERFACES

www.acsami.org

Research Article

Thermoelectric Performance Enhancement in Commercial $Bi_{0.5}Sb_{1.5}Te_3$ Materials by Introducing Gradient Cu-Doped Grain Boundaries

Shuankui Li, Wenguang Zhao, Yajuan Cheng, Lei Chen, Mengxin Xu, Kai Guo,* and Feng Pan*

Cite This: *ACS Appl. Mater. Interfaces* 2023, 15, 1167−1174

Read Online

ACCESS | Metrics & More | Article Recommendations | Supporting Information

ABSTRACT: Modulated doping has always been a conventional and effective way to optimize thermoelectric (TE) materials. Unfavorably, the efficiency of conventional doping is always restricted by the strong interdependence of thermoelectric parameters. Here, an unconventional grain boundary doping strategy is reported to solve the above problem using commercial p-type $Bi_{0.5}Sb_{1.5}Te_3$ as matrix materials. Decoupling of the three key TE parameters and large net get of the figure of merit (ZT) could be achieved in $Bi_{0.5}Sb_{1.5}Te_3$ materials by introducing the gradient Cu-doped grain boundary. A high ZT of ∼1.40 at 350 K and a superior average ZT of ∼1.24 (300−475 K) are obtained in the as-prepared samples, projecting a maximum conversion efficiency of ∼8.25% at ΔT = 200 K, which are considerably greater than those of the commercial $Bi_{0.5}Sb_{1.5}Te_3$ matrix and the traditional Cu-doped $Bi_{0.5}Sb_{1.5}Te_3$ sample. This study gives deep insights to understand the relationships between the microstructure and the carrier/phonon transport behaviors and promotes a new strategy for improving the thermoelectric performance of commercial p-type $Bi_{0.5}Sb_{1.5}Te_3$ materials.

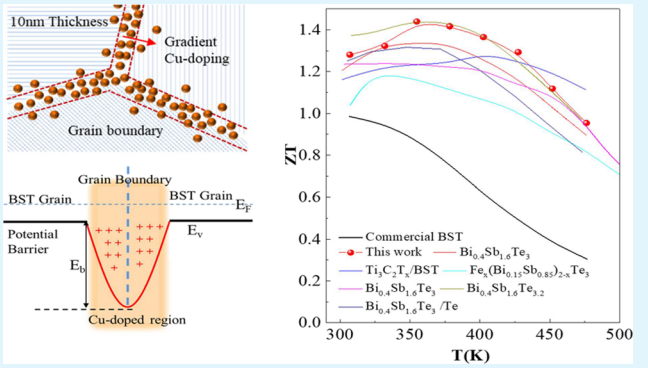

KEYWORDS: *thermoelectric, $Bi_{0.5}Sb_{1.5}Te_3$, grain boundaries, cu doping, phonon scattering, commercial material*

1. INTRODUCTION

As a potential strategy to improve the efficiency of resource utilization and achieve carbon neutrality, thermoelectric (TE) technology has drawn considerable interest recently.[1−3] The efficiency of TE conversion depends on the figure of merit (ZT) of TE materials, defined as $ZT = S^2\sigma T/\kappa_{tot}$, where S, σ, T, and κ_{tot} are the Seebeck coefficient, electrical conductivity, absolute temperature, and total thermal conductivity, respectively. Thus, an excellent TE material should possess high S, large σ, as well as low κ_{tot} simultaneously. Over the past few decades, extensive strategies such as modulation doping and microstructure engineering have been adopted to improve the performance of TE materials.[4−6] Most of these studies are based on the improvement of the power factor through carrier concentration optimization or reduction of lattice thermal conductivity (κ_{latt}) by enhancing phonon scattering, and simultaneous optimization of the electrical and thermal transport properties is a great challenge.[7−9] Therefore, developing a facile strategy to improve the performance by overcoming the interdependence of TE parameters is a core goal of TE research.[10,11]

As a classical room-temperature TE material, Bi_2Te_3-based alloys remain dominant in commercial applications for solid-state refrigeration and power generation.[12−15] The large-scale application of Bi_2Te_3-based materials is restricted by its poor TE performance and high material cost. For instance, the ZT of commercial p-type BST alloy is <1, but the material cost is about 8.63×10^5 $/W. Numerous strategies have been used to optimize TE parameters and subsequently enhance ZT values of Bi_2Te_3-based alloys, such as modulated doping, nano-engineering, and grain boundary engineering.[16−19] Cu doping has been confirmed as a general way to enhance the TE performance of p-type BTS materials, which always results in the simultaneously increasing of the power factor and thermal conductivity.[20−22] In p-type BST alloys, the Cu atoms prefer to enter the Sb sites, which could provide additional holes and enhance carrier mobility. For example, Chen et al. reported a ZT value of 1.4 at 400−500 K in BST alloys via introducing Cu doping.[10] Grain boundary engineering is effective in suppressing κ_{latt}, but it always results in the reducing σ, which

Received: October 15, 2022
Accepted: December 9, 2022
Published: December 22, 2022

might lead to a worse ZT.[23,24] Both modulation doping and grain boundary engineering focus on one part of the improvement in either electrical or thermal transport properties. Herein, we combine grain boundary engineering and Cu doping to improve TE performance of commercial BST materials via significantly enhancing phonon scattering while not hindering the electrical properties.

In this work, we adopt an unconventional grain boundary doping strategy to enhance the TE performance of the commercial BST material. Different from traditional modulated doping, decoupling of the three key TE parameters and large net get of ZT could be achieved by introducing gradient Cu-doped grain boundaries to BST materials. The introduction of gradient Cu doping at grain boundaries is beneficial for the increase of carrier concentration and carrier mobility, leading to an overall enhancement of *PF*. Meanwhile, the synergistic reduction of κ_{latt} is also achieved due to the enhanced phonon scattering, as described in Figure 1.

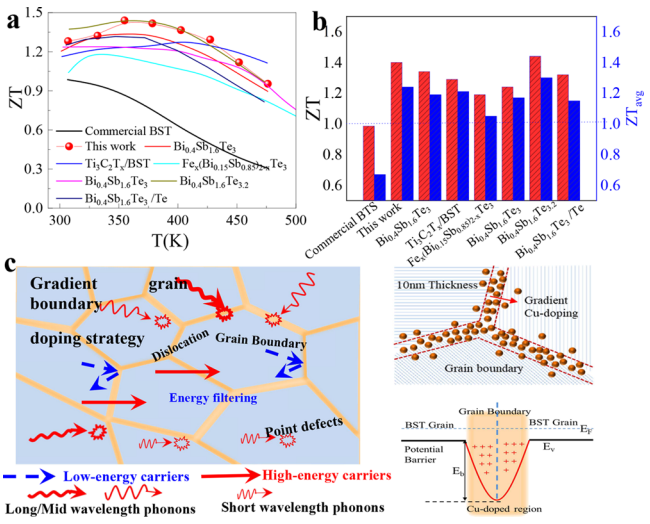

Figure 1. (a) Temperature-dependent *ZT* of the as-prepared sample. Several high-performance BST-based materials from literature data are provided for comparison. (b) ZT_{avg} and ZT_{max} in as-prepared BST-based materials. (c) Energy-filtering effect and phonon-scattering effects at the Cu-doped grain boundaries.

Benefiting from the full decoupling of TE parameters, the as-prepared samples exhibit superior TE performance to the commercial BST matrix as well as the conventional Cu-doped sample. Finally, a high *ZT* = 1.40@350 K and an average *ZT* = 1.24(300−475 K) are obtained in the optimized sample, which are about 43 and 76% higher than the corresponding values of the BTS matrix. In addition, compared with other studies, the ZT value obtained for this work shows superiority in a wide range (Figure 1a,b).[14,24−30] Finally, a maximum conversion efficiency of about ∼8.25% is achieved at Δ*T* = 200 K in the optimized material.[31,32] These results confirm that the unconventional grain boundary doping strategy is a highly effective way to decouple TE parameters, which provides a novel insight into designing high-performance TE materials.

2. EXPERIMENTAL SECTION

2.1. Materials Synthesis. The commercial BST alloy rod was purchased from Wangu Electronic materials Co., Ltd. The BST/$CuBr_2$ sample was obtained by ball-milling at a milling speed of 800 rpm for 30 min in ambient Ar. The BST/$CuBr_2$ samples with a $CuBr_2$ content of about 0.*X* wt% are noted as BCX. The as-prepared BST/$CuBr_2$ powders were immediately condensed by hot-press-sintering in a Φ10 mm graphite die at 673 K with an axial pressure of 50 MPa for 30 min. The as-prepared HD1 samples were hot-deformed (HD) in a Φ11 mm graphite die at 673 K to obtain HD2 samples. In the same way, the HD3 samples are obtained by HD of the HD2 samples in a Φ12 mm graphite die. The cuboid about 2.5 mm × 2.5 mm × 9 mm was cut along the in-plane direction to measure σ and *S*, and a square piece about 10 mm × 10 mm × 2 mm was cut along the same direction to measure the thermal conductivity, as shown in Figure S1.

2.2. Thermoelectric Measurements. The electrical conductivity and Seebeck coefficient were measured using ULVAC ZEM-3 within the temperature range 300−475 K. The total thermal conductivity (κ_{tot}) was calculated through $\kappa_{tot} = DC_p\rho$, where *D*, C_p, and ρ are the thermal diffusivity coefficient, specific heat capacity, and density, respectively. The thermal diffusivity coefficient was measured by a laser flash apparatus using Netzsch LFA 467, the specific heat (C_p) was tested by a differential scanning calorimeter (Mettler DSC1), and the density (ρ) was obtained by using the mass and dimensions of the pellet. The uncertainty of σ, *S*, and κ is estimated to be around ±3%, ±5%, and ± 5%, respectively. The combined uncertainty of the experimental determination of ZT was evaluated to be about 10−15%.

2.3. Characterization. Field-emission scanning electron microscopy (SEM) analysis of morphology and element distribution was carried out on a Zeiss SUPRA-55 microscope integrated with Oxford EDS; X-ray photoelectron spectroscopy (XPS) spectra were acquired on a Thermo Fisher ESCALAB 250X surface analysis system equipped with a monochromatized Al anode X-ray source (X-ray photoelectron spectroscopy, XPS, $h\nu$ = 1486.6 eV). The overall morphology and detailed crystallographic information are deduced from high-resolution field-emission transmission electron microscopy (FETEM; JEOL-3200FS, 300 kV). A focused ion beam system (FIB; JIB 4601F, JEOL) was used to prepare the TEM and electron backscatter diffraction (EBSD) samples of the sintered bulk sample. It should be noted that the TEM and EBSD were operated along the measuring direction of TE characteristics.

3. RESULTS AND DISCUSSION

3.1. Enhanced TE Performance by Introducing Gradient Cu-Doped Grain Boundaries. To evaluate the effects of the grain boundary doping and conventional Cu doping in the carrier/phonon transport properties, the TE properties of the as-prepared BC2 and conventional Cu doping sample (D-BST) are measured (Figure 2). It should be pointed out that the conventional Cu doping sample prepared by the solid-state reaction used commercial BST and Cu powders as starting materials. As shown in Figure 2a, both samples show decreased σ with increased temperature, demonstrating their degenerate semiconductor nature. The σ values of BC2 and D-BST are obviously higher than that of the BST matrix, which is in agreement with the previous reports.[10] In p-type BST alloys, the Cu atoms tend to substitute the Sb atoms, which results in the increase of σ due to the increased hole concentration.[10,20,33] The *S* values of BC2 (200.7 μV/K) and D-BST (213.7 μV/K) are lower than that of the BST matrix (272 μV/K), as shown in Figure 2b. Compared with the sample D-BST, the BC2 sample with gradient Cu-doped grain boundaries reveals a significantly increased σ and roughly unchanged *S*. As a result, the room-temperature power factor of the BC2 (42.3 μW/cm K^2) is about 14 and 49.5% higher than that of the D-BST (37.1 μW/cm K^2) and the BST matrix (28.3 μW/cm K^2), respectively (Figure 2c). These results indicate that the grain boundary doping strategy is more effective rather than the conventional Cu doping to optimize the electronic transport property of p-type BST alloys.

https://doi.org/10.1021/acsami.2c18575
ACS Appl. Mater. Interfaces 2023, 15, 1167−1174

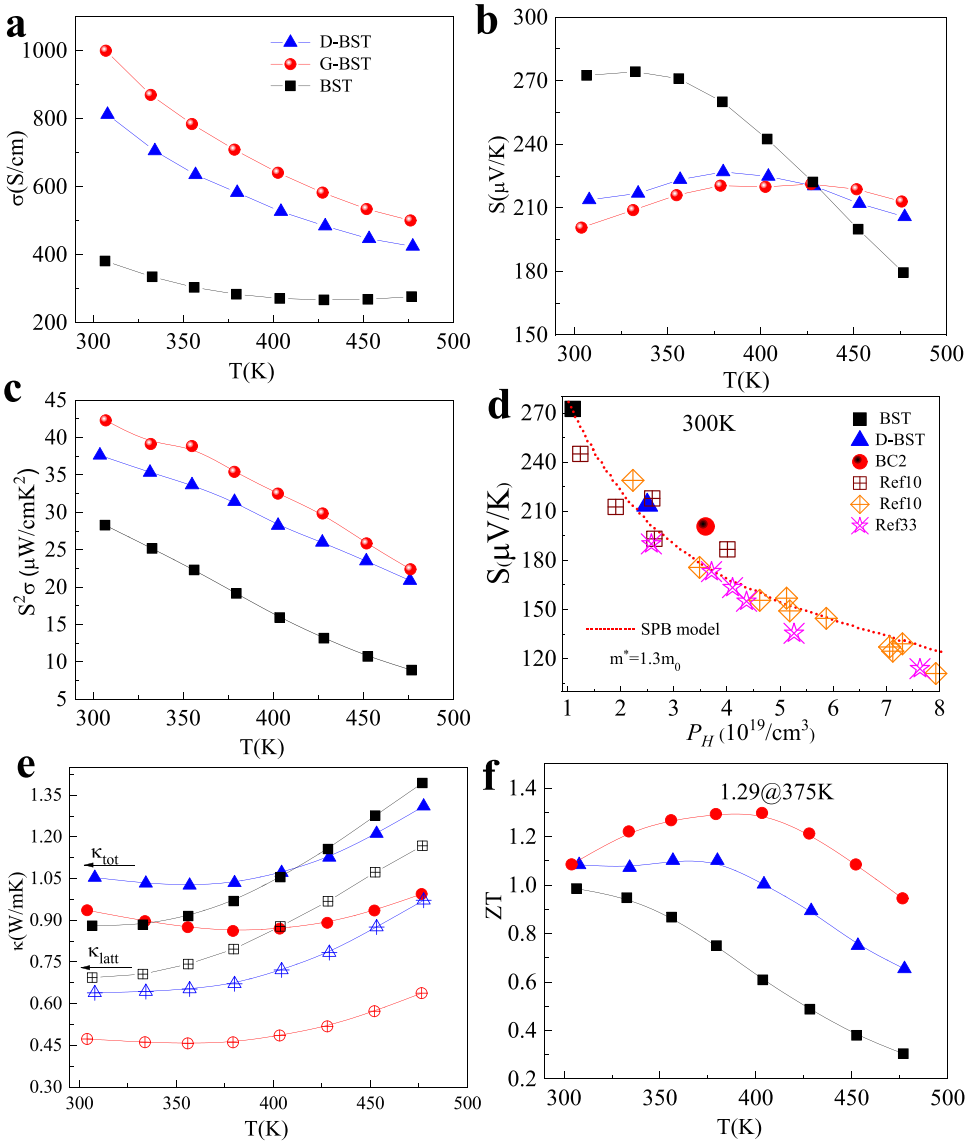

Figure 2. Comparison of thermoelectric properties of the commercial BST alloy, conventional Cu doping sample, and as-prepared BC2 sample. (a) σ, (b) S, (c) power factor, (d) S as a function of carrier concentration, (e) κ_{tot} and κ_{latt}, and (f) ZT.

To further understand the electrical properties of the as-prepared samples, the carrier concentration (n_p) and mobility at 300 K are measured and analyzed, as presented in Table S1. The measured n_p values of sample BC2 ($\sim 3.0 \times 10^{19}$ cm^{-3}) and D-BST ($\sim 2.5 \times 10^{19}$ cm^{-3}) are close, which are both significantly higher than that of the BST ($\sim 1.1 \times 10^{19}$ cm^{-3}). In BST alloys, the Cu atoms prefer to enter the Sb sites due to the small electronegativity and radius difference between Cu and Sb, which could act as an acceptor to introduce additional holes to the system.[10] At room temperature, the μ_H values for BC2 and D-BST are 209.6 cm^2 V^{-1} S^{-1} and 197.2 cm^2 V^{-1} S^{-1}, which are all higher than that of the undoped BST (182.9 cm^2 V^{-1} S^{-1}). These enhanced carrier mobilities might benefit from weakened ionized impurity scattering and acoustic phonon scattering.[10] As shown in Figure 2d, the density-of-state effective mass m^* values were estimated with an assumption of a single parabolic band model. It is obvious that the m^* value of the BC2 sample is higher than that of the D-BST and BST samples, which could be attributed to the decreased minor carrier (electron) density and weakened negative effects of minor carriers on the electrical transport properties due to Cu doping. Moreover, at the gradient Cu-doped grain boundaries, the accumulation of charges could form a potential barrier, in which charge carriers are filtered selectively.

Besides improving the electronic transport properties, the thermal transport properties could also be modulated by introducing the gradient Cu-doped grain boundaries. Figure 2e displays the κ_{tot} and κ_{latt} values of D-BST, BC, and BST samples. κ_{tot} is the sum of the electronic (κ_e) and lattice (κ_{latt}) constituents, and κ_e could be calculated by the Wiedemann–Franz law $\kappa_e = L\sigma T$, where L is the Lorenz number and is described as $L = 1.5 + \exp.(-|S|/116)$. At room temperature, the κ_{tot} values of the BC2 and D-BST are much higher than that of the BTS matrix, which is mainly due to the high κ_e. The κ_e of BC2 sample is about 0.54 W/mK, which is ≈52% of the κ_{tot}. Although the κ_{tot} values of the BC2 and D-BST are much higher than that of the BTS matrix, the κ_{latt} values are significantly reduced. According to previous reports, introducing Cu doping to BST could decrease κ_{latt} by enhancing the phonon scattering from point defects and suppressing the

https://doi.org/10.1021/acsami.2c18575
ACS Appl. Mater. Interfaces 2023, 15, 1167−1174

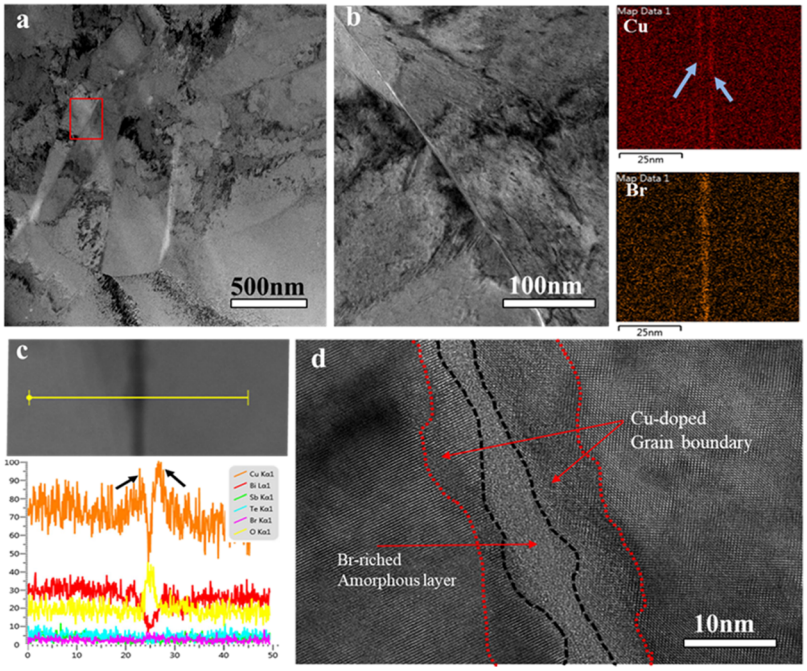

Figure 3. TEM characterizations of the as-prepared BC samples. (a) Low magnification TEM image, (b) HRTEM image and corresponding EDS elemental maps of the red rectangular region in (a). (c) EDS line mapping and (d) HRTEM image of gradient Cu-doped grain boundaries.

contribution of minor carrier concentrations (electrons).[10,34] In the present work, the κ_{latt} of the BC2 (0.5 W/mK) is 21.9% lower than that of D-BST (0.64 W/mK), which could be ascribed to the enhanced phonon scattering at Cu-doped grain boundaries. Consequently, the maximum ZT reaches ~1.29 at 375 K, and a prominent average ZT of ~1.18 (350~475 K) is attained in the BC2 sample, which shows superiority when compared with that of D-BST and BST (Figure 2e). It is obvious that the improved power factor and greatly reduced thermal conductivity were simultaneously achieved in the BC2 sample, which could be ascribed to the introduced gradient Cu-doped grain boundaries.

3.2. Microstructures of the Cu-Doped Grain Boundaries. The microstructure of the BC sample is further studied by TEM. As shown in Figure 3a, the grains of BC are closely packed and the sizes are from hundreds of nanometers to several microns. Figure 3b shows the typical HRTEM image of two neighboring grains with a clear grain boundary. The corresponding EDS analysis across grain boundary shows the Cu- and Br-rich complexes compared with the matrix regions. It is noted that the obvious $CuBr_2$ precipitate is not observed in the sample. The magnified TEM image and EDS line scans (Figure 3b,c) reveal that the sandwich-like grain boundary with a thickness of about 10−15 nm is formed. The Br-rich amorphous layer with a thickness of about 2~5 nm could be observed clearly, which originates from the reaction between the $CuBr_2$ and BTS matrix during the HD process. Moreover, due to the diffusion of Cu^{2+} ions from the BTS grain surface to the inside, the gradient Cu-doped grain boundary is formed, which could be clearly observed in the HRTEM and EDS line scans (Figure 3c,d). It is found that the total thickness of the Cu-doped grain boundaries layer is about 5−10 nm. Various and abundant atomic-scale distortions are unveiled at the grain boundaries, such as point defects, tiny distorted regions, dislocations, and strain field domains. Thus, in BC samples, Cu doping ensured the high carrier concentration, and the potential barriers at grain boundaries contribute to the high carrier mobility and the Seebeck coefficient. Above discussion is consistent with the results that although the n_p value of BC is higher than that of D-BST, the Seebeck coefficient is roughly unchanged. Moreover, a large number of grain boundaries and atomic-scale distortions in the sample can significantly enhance the scattering of phonons with various wavelengths and reduce κ_{latt}. Therefore, the simultaneous optimization of the carrier and phonon transport properties has been achieved in the present work by introducing gradient Cu-doped grain boundaries to the commercial BST material.

3.3. Enhancing the TE Performance by the HD Process. In this work, the formation of Cu-doped grain boundaries originates from the reaction between the $CuBr_2$ and BTS matrix during the HD process. Due to the relatively low melting point and hardness, the added $CuBr_2$ secondary phase could be squeezed to the newly formed grain boundaries, which is crucial to regulate the microstructure of the sample. Thus, a multiple HD process is employed to further improve the TE performance of BC samples. Figure 4a,b presents electronic transport properties of the BC2 samples subjected to the multiple HD process, which reveals that the trade-off between σ and S could be broken via the multiple HD process. Both σ and S increased with the increasing HD number, which may be attributed to the increased density of Cu-doped grain boundaries. In particular, σ (~999.3 S/cm) and S (205.7 μV/K) at 300 K for BC2−3 increased by 10.9 and 6.8% compared to those of BC2−1 (~900.9 S/cm and 192.6 μV/K), respectively. Finally, the power factor of BC2−3 is about ~42.3 μW/cm K^2 at 300 K, which is about ~26.6% higher than that of the BC2−1 (~33.4 μW/cm K^2). Subsequently, the thermal transport properties are modulated by the HD process. As shown in Figure 4c. κ_{tot} is increased slightly with the increasing HD number. After excluding κ_e, the κ_{latt} is also slightly increased after the HD process. Typically, the κ_{latt} of 0.53 W/mK at 300 K is achieved

https://doi.org/10.1021/acsami.2c18575
ACS Appl. Mater. Interfaces 2023, 15, 1167−1174

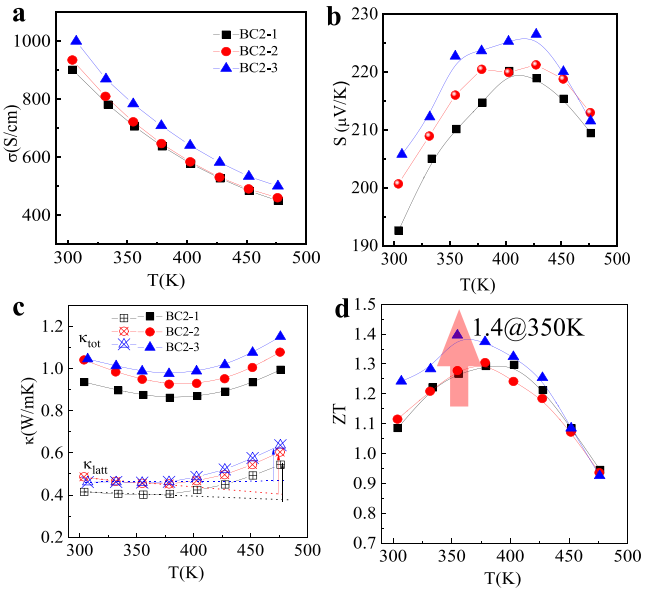

Figure 4. Thermoelectric properties of the as-prepared BC2 samples with different HD numbers. (a) σ, (b) S, (c) κ_{tot} and κ_{latt}, and (d) ZT value.

in the BC2−3, which increased by approximately 13% compared with that of BC2−1. As a result, the ZT values are effectively enhanced by the multiple HD process, as shown in Figure 4d. The maximum ZT is about 1.40 at 350 K, increased by 10% as compared with that of BC2−1. The average ZT reached as high as ∼1.24 between 300 and 475 K, which is 6% higher than that of BC2−1. It should be noted that for the commercial BST matrix, the TE performance has no obvious change with the increased HD number, further confirming that the Cu-doped grain boundary is essential to improve the TE performance of the BC sample (Figure S2).

3.4. Microstructure Evolution during the HD Process. To quantitatively investigate the microstructure evolution of the sample during the HD process, the EBSD characterization is performed. As shown in Figure 5a, the BC-1 sample exhibited randomly oriented grains with an average grain size of about 1.8 μm. With the increasing HD number, the average grain size decreased slightly due to the fragmentation of grains, as shown in Figure 5b. The average grain size of the BC2−3 is about 0.8 μm, which decreased by approximately 56% compared with that of BC2−1. As shown in EBSD images (Figures S3 and S4), a few large grains with a laminar structure appeared, which could be observed in the sample after the HD process. This result means the recrystallization of BST grains occurred during the HD process, which lead to the increased κ_{latt}. The above discussion is consistent with the experimental results that the κ_{latt} of BC2−3 is higher than that of BC2−1. XPS spectra of Cu 2p confirm the existence of Cu^{2+} ions in the BC samples. For the sample after the HD process, the locations of Cu 2p peaks have no obvious shift, indicating that the valence of Cu^{2+} ions is not changed (Figure 5c). Furthermore, TEM observations are conducted to investigate the microstructure evolution during the HD process. As shown in Figures 5d and S5, many nano-sized $CuBr_2$ particles are observed in the BC2−1 sample and mainly located at the boundary of BST grains. During the HD process, the $CuBr_2$ secondary phase could be squeezed to the grain boundaries, and the Cu-doped grain boundary could be formed. The above discussion is in accordance with the TEM results that the CuBr2 particles at the grain boundary are gradually diminished with increasing HD numbers (Figures 5e,f). Therefore, by applying the multiple HD process using $CuBr_2$ as the interface modification material, the Cu-doped grain boundary is introduced to the commercial BST material.

3.5. Compositional Optimization of BC Samples. As mentioned above, the $CuBr_2$ content is essential to the TE performance of the as-prepared BC sample, As shown in Figure 6, σ, PF, κ_{latt}, and ZT at 300 K as functions of the $CuBr_2$ content for the BC samples with different HD numbers are displayed. Almost for all samples with different $CuBr_2$ contents, σ increased with the increase of the HD number (Figure S6). The increased σ originates from the diffusion of Cu^{2+} ions at the BTS grain boundaries as well as the recrystallization of BST grains during the HD process. Therefore, the PF values are extremely increased with the increase of the HD number, as shown in Figure S6. For samples with the same HD number, the σ increased significantly with the increase of the $CuBr_2$ content and tended to saturate with a high $CuBr_2$ content (>0.1 wt %) (Figures 6a and S7). Obviously, the BC2 samples

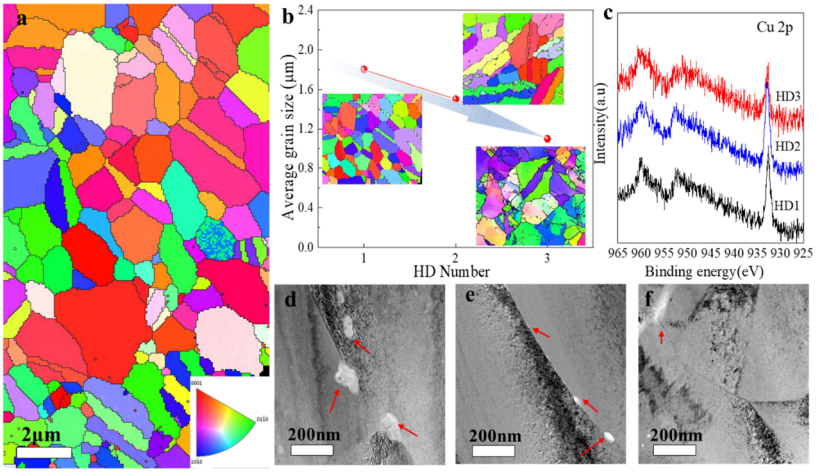

Figure 5. (a) EBSD maps of the as-prepared BC sample. (b) Grain size of the sample varies with the HD number and the inset of (b) is the corresponding EBSD maps. (c) XPS spectra of Cu 2p peaks for the samples with different HD numbers. Typical HRTEM image at grain boundaries for samples (d) BC-1, (e) BC-2, and (f) BC-3.

https://doi.org/10.1021/acsami.2c18575
ACS Appl. Mater. Interfaces 2023, 15, 1167−1174

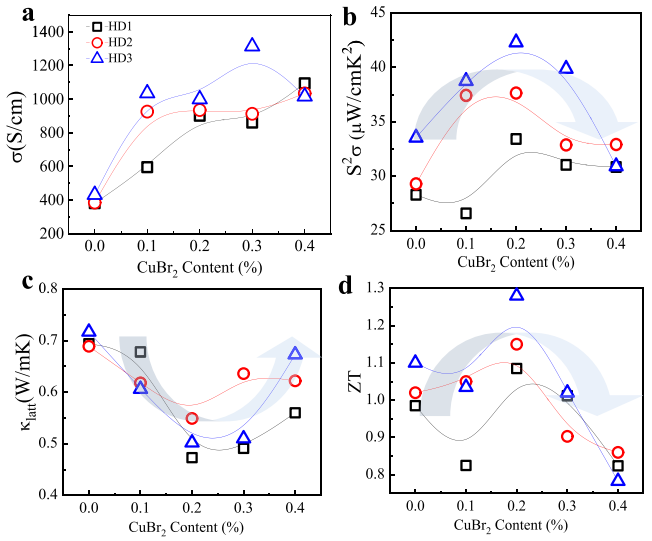

Figure 6. TE properties at 300 K of the as-prepared BC samples. Variations of (a) σ, (b) *PF*, (c) κ_{latt}, and (d) *ZT* as a function of the $CuBr_2$ content.

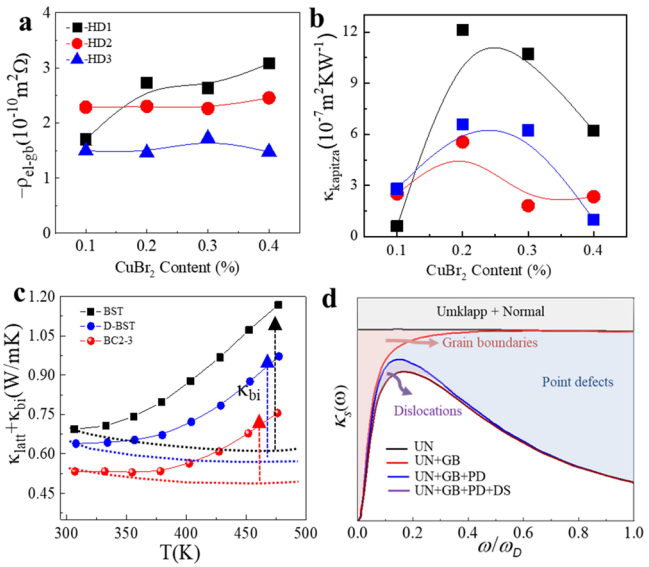

Figure 7. (a) Interfacial electrical resistance ($\rho_{el\text{-}gb}$) and (b) interfacial thermal resistance ($\kappa_{Kapitza}$) at 300 K of the as-prepared BC samples calculated using the two-phase model. (c) Experimental and calculated data of the commercial BST alloy, conventional Cu doping sample, and as-prepared BC2 sample. (d) Frequency-dependent spectral lattice thermal conductivity of BC2−3 calculated using the Debye−Callaway model.

have maximum *PF* values (Figures 6b and S8). Moreover, the thermal transport properties of the samples with different $CuBr_2$ contents are presented in Figures S9 and S10. For samples with the same HD number, the κ_{tot} at 300 K increased significantly with the increase of the $CuBr_2$ content due to the increased κ_e (Figure S11). As shown in Figure 6c, the κ_{latt} of as-prepared samples could be obtained by excluding κ_e from κ_{tot}. The introduction of $CuBr_2$ results in an initial drop ($CuBr_2$ content <0.2%) and then rise ($CuBr_2$ content ≥ 0.2%) trend with the increasing $CuBr_2$ content. At a low $CuBr_2$ content (<0.2%), the κ_{latt} slightly decreased with the increase of the HD number. As mentioned above, the massively increased grain boundary density due to the grain size decrease from 1.8 to 0.8 μm is the main reason for the reduction of κ_{latt}. For the samples with a high $CuBr_2$ content (≥0.2%), the κ_{latt} increased with the increasing HD number due to the recrystallization of BST grains as well as the diffusion of Cu^{2+} ions during the HD process. Specially, the maximum ZT of 1.28 at 300 K is attained for BC2−3 (Figure 6d), about 18.5 and 30.6% increment as compared to the BC2−1 and commercial BST, respectively.

3.6. Effects of the Gradient Cu-Doped Grain Boundary to the Phonon/Carrier Transport Behaviors. For the polycrystalline bulk TE material, grain boundaries play multiple roles in the phonon/carrier transportation. Under normal conditions, the grain boundary acts as a potential barrier, which leads to an interfacial resistance due to the energy-filtering effect.[23,34,35] In the present work, the energy filtering as well as Cu doping at the grain boundary all affect the electron transport behaviors of the as-prepared sample. Thus, the two-phase model consisting of the grain phase and the grain boundary phase is used to analyze the carrier/phonon transport behaviors of the as-prepared sample.[36,37] The additional interfacial electrical resistance originated from the gradient Cu-doped grain boundary ($\rho_{ad\text{-}gb}$) is estimated, as shown in Figure 7a. It is noted that in the present work, the calculated $\rho_{ad\text{-}gb}$ values are negative, implying that the introduced gradient Cu-doped grain boundary benefits the increase of σ. Moreover, the absolute value of $\rho_{ad\text{-}gb}$ decreased after the HD process, which could be ascribed to the decreasing of grain boundary layer thickness as well as the diffusion of Cu^{2+} ions from grain boundaries to BTS grains. Typically, the absolute value of $\rho_{ad\text{-}gb}$ for BC2−1 is about 2.73 × 10^{-10} $m^2\Omega$, nearly 1.9 times greater than that of BC2−3 (1.45 × 10^{-10} m^2 Ω). The interfacial thermal resistance ($\kappa_{Kapitza}$) originated from the gradient Cu-doped grain boundary ($\rho_{ad\text{-}gb}$) is also estimated, as shown in Figure 7b. After the HD process, the $\kappa_{Kapitza}$ decreased from 12.11 × 10^{-7} m^2 kW^{-1} (BC2−1) to 6.57 × 10^{-7} m^2 kW^{-1} (BC2−1), which could be attributed to the enhanced phonon scattering at Cu-doped grain boundaries. Thus, in the as-prepared sample, the Cu dopants at grain boundaries benefit the increase of electrical conductivity, and the atomic defects and grain boundaries act as the extra phonon scattering centers that result in the additional interfacial thermal resistance.

The Debye−Callaway model is adopted to analyze the contribution of the various phonon-scattering mechanisms to the reduction of κ_{latt} in the as-prepared sample. By taking account of the various phonon-scattering mechanisms including the Umklapp process, point defects, grain boundaries, and dislocation cores, the calculated results agree well with the experimental data at a low-temperature range. At a high-temperature range, the calculated results deviated from experimental data due to the thermally excited bipolar effect. As shown in Figure 7c, the κ_{bi} values of D-BST and BC are much lower than that of BST, which is consistent with the reported results that doping Cu into the BST could effectively suppress the κ_{bi} via reducing minor carrier concentrations. Moreover, the calculated frequency-dependent phonon scattering process is also present in Figure 7d. The result suggests that the introduced point defects scattered high-frequency phonons, the dislocation and nanostructures scattered middle-frequency phonons, and the abundant grain boundaries scattered low-frequency phonons.[38,39] Therefore, the low κ_{latt} in the as-prepared sample can be attributed to the combination

https://doi.org/10.1021/acsami.2c18575
ACS Appl. Mater. Interfaces 2023, 15, 1167−1174

phonon scattering effects of multiscale hierarchical scattering architectures.[40−42]

In summary, the Cu-doped grain boundaries significantly minimize the κ_{latt} by enhancing phonon scattering and simultaneously enhance *PF* due to breaking trade-off between σ and S. Benefiting from the decoupling of the TE parameters, the maximum and average ZT values of 1.4 and 1.24 are achieved in the optimized sample, which are 56 and 63% higher than those of commercial BST ingots, respectively. These results demonstrate that the grain boundary doping strategy has great advantages compared to the conventional doping methods, which can open up exciting possibilities in developing high-performance TE materials. Meanwhile, considering the simple synthesis process and using commercial BST ingots, the present strategy has great realistic application potential. Furthermore, the further prospect of this study is introducing other low melting chemical compounds (such as $ZnBr_2$ and CuBr) and further extending the strategy to other TE material systems.

4. CONCLUSIONS

In summary, an unconventional grain boundary doping strategy is employed to enhance the TE performance of the commercial BST material. The gradient Cu-doped grain boundaries significantly minimize the κ_{latt} value by enhancing phonon scattering and simultaneously enhance *PF* due to breaking trade-off between σ and *S*. Benefiting from the decoupling of the TE parameters, a high ZT of ∼1.40 at 350 K and a superior average ZT of ∼1.24 (300−475 K) are obtained in the optimized sample, projecting a maximum conversion efficiency of ∼8.25% at ΔT = 200 K. These results are much superior to those of the commercial BST matrix and traditional Cu-doped BST. The present work not only attests the efficacy of grain boundary engineering in TE materials but also brings out a new avenue for conventional modulation doping. Our work presents a simple and effective strategy to improve the TE performance of the commercial p-type BST material, which has high industrial compatibility and great realistic application potential.

■ ASSOCIATED CONTENT

Supporting Information

The Supporting Information is available free of charge at https://pubs.acs.org/doi/10.1021/acsami.2c18575.

Details of the thermoelectric performance test; thermoelectric properties of commercial P-type $Bi_{0.5}Sbe_{1.5}Te_3$ thermoelectric materials; EBSD maps of BC2−2 and BC2−3; TEM characterizations of the as-prepared BC2−1 sample; thermoelectric performance of all the samples; and parameters for the calculation of lattice thermal conductivity via the Debye−Callaway model (PDF)

■ AUTHOR INFORMATION

Corresponding Authors

Kai Guo − *School of Physics and Materials Science, Guangzhou University, Guangzhou 510006, PR China;* orcid.org/0000-0002-8486-4185; Email: kai.guo@gzhu.edu.cn

Feng Pan − *School of Advanced Materials, Peking University Shenzhen Graduate School, Shenzhen 518055, China;* orcid.org/0000-0002-8216-1339; Email: panfeng@pkusz.edu.cn

Authors

Shuankui Li − *School of Physics and Materials Science, Guangzhou University, Guangzhou 510006, PR China*

Wenguang Zhao − *School of Advanced Materials, Peking University Shenzhen Graduate School, Shenzhen 518055, China*

Yajuan Cheng − *School of Physics and Materials Science, Guangzhou University, Guangzhou 510006, PR China*

Lei Chen − *School of Physics and Materials Science, Guangzhou University, Guangzhou 510006, PR China*

Mengxin Xu − *Institute of Modern Physics, Chinese Science Academy, Lanzhou, Gansu 730030, China*

Complete contact information is available at: https://pubs.acs.org/10.1021/acsami.2c18575

Author Contributions

The manuscript was written through contributions of all authors. All authors have given approval to the final version of the manuscript. S.L. and W.Z. contributed equally to this work.

Funding

The work was financially supported by the National Natural Science Foundation of China (No. 21905007) and Guangdong Basic and Applied Basic Research Foundation (2019A1515010832).

Notes

The authors declare no competing financial interest.

■ REFERENCES

(1) Mao, J.; Chen, G.; Ren, Z. F. Thermoelectric Cooling Materials. *Nat. Mater.* **2021**, *20*, 454−461.

(2) Bell, L. E. Cooling, Heating, Generating Power, and Recovering Waste Heat with Thermoelectric Systems. *Science* **2008**, *321*, 1457.

(3) Gayner, C.; Amouyal, Y. Energy Filtering of Charge Carriers: Current Trends, Challenges, and Prospects for Thermoelectric Materials. *Adv. Funct. Mater.* **2020**, *30*, No. 1901789.

(4) Li, S.; Xin, C.; Liu, X.; Feng, Y.; Liu, Y.; Zheng, J.; Liu, F.; Huang, Q.; Qiu, Y.; He, J.; Luo, J.; Pan, F. 2D Hetero-nanosheets to Enable Ultralow Thermal Conductivity by All Scale Phonon Scattering for Highly Thermoelectric Performance. *Nano Energy* **2016**, *30*, 780−789.

(5) Tan, M.; Shi, X.; Liu, W.; Li, M.; Wang, Y.; Li, H.; Deng, Y.; Chen, Z. Synergistic Texturing and Bi/Sb-Te Antisite Doping Secure High Thermoelectric Performance in $Bi_{0.5}Sb_{1.5}Te_3$-Based Thin Films. *Adv. Energy Mater.* **2021**, *11*, No. 2102578.

(6) Shi, X.; Zou, J.; Chen, Z. Advanced Thermoelectric Design: From Materials and Structures to Devices. *Chem. Rev.* **2020**, *120*, 7399−7515.

(7) Xiao, C.; Li, Z.; Li, K.; Huang, P.; Xie, Y. Decoupling Interrelated Parameters for Designing High Performance Thermoelectric Materials. *Acc. Chem. Res.* **2014**, *47*, 1287−1295.

(8) Zhi, S.; Jia, J.; Zhang, Q.; Cao, F.; Liu, X.; Mao, J. A Sketch for Super-thermoelectric Materials. *Mater. Today Phys.* **2022**, *22*, No. 100618.

(9) Novak, T. G.; Kim, K.; Jeon, S. 2D and 3D Nanostructuring Strategies for Thermoelectric Materials. *Nanoscale* **2019**, *11*, 19684.

(10) Hao, F.; Qiu, P.; Song, Q.; Chen, H.; Lu, P.; Ren, D.; Shi, X.; Chen, L. Roles of Cu in the Enhanced Thermoelectric Properties in $Bi_{0.5}Sb_{1.5}Te_3$. *Materials* **2017**, *10*, 251.

(11) Hao, F.; Qiu, P.; Tang, Y.; Bai, S.; Xing, T.; Chu, H. S.; Zhang, Q.; Lu, P.; Zhang, T.; Ren, D.; Chen, J.; Shi, X.; Chen, L. High Efficiency Bi_2Te_3-based Materials and Devices for Thermoelectric

Power Generation between 100 and 300 °C. *Energy Environ. Sci.* **2016**, *9*, 3120−3127.
(12) Li, S.; Liu, Y.; Liu, F.; He, D.; He, J.; Luo, J.; Xiao, Y.; Pan, F. Effective Atomic Interface Engineering in $Bi_2Te_{2.7}Se_{0.3}$ Thermoelectric Material by Atomic-layer-deposition Approach. *Nano Energy* **2018**, *49*, 257−266.
(13) Zhu, B.; Wang, W.; Cui, J.; He, J. Point Defect Engineering: Co-Doping Synergy Realizing Superior Performance in n-Type Bi_2Te_3 Thermoelectric Materials. *Small* **2021**, *17*, No. 2101328.
(14) Pan, Y.; Qiu, Y.; Witting, I.; Zhang, L.; Fu, C.; Li, J.-W.; Huang, Y.; Sun, F.-H.; He, J.; Snyder, G. J.; Felser, C.; Li, J.-F. Synergistic Modulation of Mobility and Thermal Conductivity in $(Bi,Sb)_2Te_3$ towards High Thermoelectric Performance. *Energy Environ. Sci.* **2019**, *12*, 624−630.
(15) Li, S.; Wang, R.; Zhu, W.; Chu, M.; Huang, Z.; Zhang, Y.; Zhao, W.; Liu, F.; Luo, J.; Xiao, Y.; Pan, F. Achieving High Thermoelectric Performance by Introducing 3D Atomically Thin Conductive Framework in Porous $Bi_2Te_{2.7}Se_{0.3}$-Carbon Nanotube Hybrids. *Adv. Electron. Mater.* **2020**, *6*, No. 2000292.
(16) Yu, B.; Duan, J.; Cong, H.; Xie, W.; Liu, R.; Zhuang, X.; Wang, H.; Qi, B.; Xu, M.; Wang, Z.; Zhou, J. Thermosensitive crystallization-boosted liquid thermocells for low-grade heat harvesting. *Science* **2020**, *370*, 342−346.
(17) Tan, M.; Liu, W.; Shi, X.; Shang, J.; Li, H.; Liu, X.; Kou, L.; Dargusch, M.; Deng, Y.; Chen, Z. In situ Crystal-amorphous Compositing inducing Ultrahigh Thermoelectric Performance of p-type $Bi_{0.5}Sb_{1.5}Te_3$ Hybrid Thin Films. *Nano Energy* **2020**, *78*, No. 105379.
(18) Chen, W.; Shi, X.; Zou, J.; Chen, Z. Thermoelectric Coolers for On-chip Thermal Management: Materials, Design, and Optimization. *Mater. Sci. Eng., R* **2022**, *151*, No. 100700.
(19) Cao, T.; Shi, X.; Chen, Z. Advances in the Design and Assembly of Flexible Thermoelectric Device. *Prog. Mater. Sci.* **2023**, *131*, No. 101003.
(20) Kim, Y.-M.; Lee, K. H.; Fu, L.; Oh, M.-W.; Yang, S.-H.; Ning, S.; Han, G.; Kim, M. Y.; Kim, J.-S.; Jeong, M.; Jang, J.; Lee, E.; Okunishi, E.; Sawada, E.; Kim, H. S.-I.; Pennycook, S. J.; Lee, Y. H.; Kim, S. W. Atomic-scale Chemical Mapping of Copper Dopants in $Bi_2Te_{2.7}Se_{0.3}$ Thermoelectric Alloy. *Mater. Today Phys.* **2021**, *17*, No. 100347.
(21) Chen, T.; Chen, Q.; Schouteden, K.; Huang, W.; Wang, X.; Li, Z.; Miao, F.; Wang, X.; Li, Z.; Zhao, B.; Li, S.; Song, F.; Wang, J.; Wang, B.; Haesendonck, C. V.; Wang, G. Topological Transport and Atomic Tunnelling−clustering Dynamics for Aged Cu-doped Bi_2Te_3 crystals. *Nat. Commun.* **2014**, *5*, 5022.
(22) Lim, Y. S.; Song, M.; Lee, S.; An, T. H.; Park, C.; Seo, W. S. Enhanced Thermoelectric Properties and Their Controllability in p-type $(BiSb)_2Te_3$ Compounds through Simultaneous Adjustment of Charge and Thermal Transports by Cu Incorporation. *J. Alloys Compd.* **2016**, *687*, 320−325.
(23) Li, S.; Huang, Z.; Wang, R.; Zhao, W.; Luo, J.; Xiao, Y.; Pan, F. Highly Distorted Grain Boundary with an Enhanced Carrier/Phonon Segregation Effect Facilitates High-Performance Thermoelectric Materials. *ACS Appl. Mater. Interfaces* **2021**, *13*, 51018−51027.
(24) Lu, X.; Zhang, Q.; Liao, J.; Chen, H.; Fan, Y.; Xing, J.; Gu, S.; Huang, J.; Ma, J.; Wang, J.; Wang, L.; Jiang, W. High-Efficiency Thermoelectric Power Generation Enabled by Homogeneous Incorporation of MXene in $(Bi,Sb)_2Te_3$ Matrix. *Adv. Energy Mater.* **2020**, *10*, No. 1902986.
(25) Cai, B.; Zhuang, H.; Pei, J.; Su, B.; Li, J.; Hu, H.; Jiang, Y.; Li, J. Spark Plasma Sintered Bi-Sb-Te Alloys derived from Ingot Scrap: Maximizing Thermoelectric Performance by tailoring Their Composition and Optimizing Sintering Time. *Nano Energy* **2021**, *85*, No. 106040.
(26) Li, C.; Ma, S.; Cui, W.; Sang, X.; Wei, P.; Zhu, W.; Nie, X.; Zhao, W.; Zhang, Q. Magnetoresistance-enhanced Electro-thermal Conversion Performance. *Mater. Today Phys.* **2021**, *19*, No. 100409.
(27) Pei, J.; Dong, J.; Cai, B.; Zhang, Y.; Zhou, W.; Zhang, B.-P.; Ge, Z.-H.; Li, J.-F. Weak-Ferromagnetism for Room Temperature Thermoelectric Performance Enhancement in p-type $(Bi, Sb)_2Te_3$. *Mater. Today Phys.* **2021**, *19*, No. 100423.
(28) Nozariasbmarz, A.; Poudel, B.; Li, W.; Kang, H. B.; Zhu, H.; Priya, S. Bismuth Telluride Thermoelectrics with 8% Module Efficiency for Waste Heat Recovery Application. *iScience* **2020**, *23*, No. 101340.
(29) Zhuang, H.; Pei, J.; Cai, B.; Dong, J.; Hu, H.; Sun, F.; Pan, Y.; Snyder, G. J.; Li, J. Thermoelectric Performance Enhancement in BiSbTe Alloy by Microstructure Modulation via Cyclic Spark Plasma Sintering with Liquid Phase. *Adv. Funct. Mater.* **2021**, *31*, No. 2009681.
(30) Yang, G.; Niu, R.; Sang, L.; Liao, X.; Mitchell, D. R. G.; Ye, N.; Pei, J.; Li, J.; Wang, X. Ultra-High Thermoelectric Performance in Bulk BiSbTe/Amorphous Boron Composites with Nano-Defect Architectures. *Adv. Energy Mater.* **2020**, *10*, No. 2000757.
(31) Snyder, G. J.; Snyder, A. H. Figure of merit ZT of a Thermoelectric Device Defined from Materials Properties. *Energy Environ. Sci.* **2017**, *10*, 2280.
(32) Zhu, B.; Liu, X.; Wang, Q.; Qiu, Y.; Shu, Z.; Guo, Z.; Tong, Y.; Cui, J.; Gu, M.; He, J. Realizing Record High Performance in n-type Bi_2Te_3-based Thermoelectric Materials. *Energy Environ. Sci.* **2020**, *13*, 2106−2114.
(33) Shi, Q.; Chen, X.; Chen, Y.; Zhao, X.; He, W.; Zhou, C.; Ang, R. Broadening Temperature Plateau of High zTs in PbTe doped $Bi_{0.3}Sb_{1.7}Te_3$ Through Defect Carrier Regulation and Multi-scale Phonon Scattering. *Mater. Today Phys.* **2022**, *22*, No. 100610.
(34) Wang, X.; He, H.; Yin, L.; Cheng, J.; Sui, J.; Liu, X.; Mao, J.; Cao, F.; Zhang, Q. Infinite Coordination Polymer for Enhancing the Thermoelectric Performance of $Bi_{0.5}Sb_{1.5}Te_3$ for Low-grade Waste Heat Recovery. *Mater. Today Energy* **2022**, *26*, No. 100994.
(35) Zide, J. M. O.; Vashaee, D.; Bian, Z. X.; Zeng, G.; Bowers, J. E.; Shakouri, A.; Gossard, A. C. Demonstration of Electron Filtering to Increase the Seebeck Coefficient in $In_{0.53}Ga_{0.47}As/In_{0.53}$ $Ga_{0.28}Al_{0.19}$ As Superlattices. *Phys. Rev. B* **2006**, *74*, No. 205335.
(36) Nan, C.-W.; Birringer, R.; Clarke, D. R.; Gleiter, H. Effective Thermal Conductivity of Particulate Composites with Interfacial Thermal Resistance. *J. Appl. Phys.* **1997**, *81*, 6692−6699.
(37) Lin, Y.; Wood, M.; Imasato, K.; Kuo, J. J.; Lam, D.; Mortazavi, N.; Slade, T. J.; Hodge, S. A.; Xi, K.; Kanatzidis, M. G.; Clarke, D. R.; Hersam, M. C.; Snyder, G. J. Expression of Interfacial Seebeck Coefficient through Grain Boundary Engineering with Multi-layer Graphene Nanoplatelets. *Energy Environ. Sci.* **2020**, *13*, 4114−4121.
(38) Chen, B.; Li, J.; Wu, M.; Hu, L.; Liu, F.; Ao, W.; Li, Y.; Xie, H.; Zhang, C. Simultaneous Enhancement of the Thermoelectric and Mechanical Performance in One-Step Sintered n-Type Bi_2Te_3-Based Alloys via a Facile MgB_2 Doping Strategy. *ACS Appl. Mater. Interfaces* **2019**, *11*, 45746−45754.
(39) Zeier, W. G.; Zevalkink, A.; Gibbs, Z. M.; Hautier, G.; Kanatzidis, M. G.; Snyder, G. J. Thinking Like a Chemist: Intuition in Thermoelectric Materials. *Angew. Chem., Int. Ed.* **2016**, *55*, 2−18.
(40) Xu, Z.; Wu, H.; Zhu, T.; Fu, C.; Liu, X.; Hu, L.; He, J.; Zhao, X. Attaining High Mid-Temperature Performance in $(Bi,Sb)_2Te_3$ Thermoelectric Materials via Synergistic Optimization. *NPG Asia Mater.* **2016**, *8*, 302.
(41) Li, S.; Zhu, W.; Xiao, Y.; Pan, F. Improving the Performance of Thermoelectric Materials by Atomic Layer Deposition-based Grain Boundary Engineering. *Chin. J. Struct. Chem.* **2020**, *39*, 831−837.
(42) Li, Y.; Weng, T.; Li, P.; Huang, H.; He, X.; Guo, K.; Zhang, J.; Xing, J.; Li, S.; Jiang, Y.; Luo, J. Improved Thermal Stability and Enhanced Thermoelectric Properties of p-Type $BaCu_2Te_2$ by Doping of Cl. *ACS Appl. Mater. Interfaces* **2022**, *14*, 5634−5642.

https://doi.org/10.1021/acsami.2c18575
ACS Appl. Mater. Interfaces 2023, 15, 1167−1174